

Discovery of two-dimensional Dirac nodal line fermions

Baojie Feng,¹ Botao Fu,² Shusuke Kasamatsu,¹ Suguru Ito,¹ Peng Cheng,³ Cheng-Cheng Liu,² Sanjoy K. Mahatha,⁴ Polina Sheverdyaeva,⁴ Paolo Moras,⁴ Masashi Arita,⁵ Osamu Sugino,¹ Tai-Chang Chiang,⁶ Kehui Wu,³ Lan Chen,^{3,*} Yugui Yao,^{2,†} and Iwao Matsuda^{1,‡}

¹*Institute for Solid State Physics, The University of Tokyo, Kashiwa, Chiba 277-8581, Japan*

²*Beijing Key Laboratory of Nanophotonics and Ultrafine Optoelectronic Systems,
School of Physics, Beijing Institute of Technology, Beijing 100081, China*

³*Institute of Physics, Chinese Academy of Sciences, Beijing 100190, China*

⁴*Istituto di Struttura della Materia, Consiglio Nazionale delle Ricerche, I-34149 Trieste, Italy*

⁵*Hiroshima Synchrotron Radiation Center, Hiroshima University,
2-313 Kagamiyama, Higashi-Hiroshima 739-0046, Japan*

⁶*Department of Physics, University of Illinois, Urbana, IL 61801, USA*

(Dated: December 9, 2024)

Topological nodal line semimetals, a novel quantum state of materials, possess topologically nontrivial valence and conduction bands that touch at a line near the Fermi level[1–3]. The exotic band structures can lead to various novel properties, such as long-range Coulomb interaction[4] and flat Landau levels[5]. Recently, topological nodal lines have been observed in several bulk materials, such as PtSn₄[6], ZrSiS[9, 10], TlTaSe₂[8] and PbTaSe₂[7]. However, in two-dimensional materials, experimental research is still lacking. Here, we report the discovery of two-dimensional Dirac nodal line fermions in monolayer Cu₂Si based on combined theoretical calculations and angle-resolved photoemission spectroscopy (ARPES) measurements. The Dirac nodal lines in Cu₂Si form two concentric loops centred around the Γ point and are protected by mirror reflection symmetry. Our results establish Cu₂Si as a new platform to study the novel physical properties in two-dimensional Dirac materials and provide new opportunities to realize high-speed low-dissipation devices.

The discovery of topological insulators has ignited great research interest in the novel physical properties of topological materials in the past decade[11, 12]. A characteristic feature of topological insulators is the existence of topologically nontrivial surface states that are protected by time reversal or crystallographic symmetries. Recently, tremendous research interest has moved from traditional topological insulators to topological semimetals which have vanishing densities of states at the Fermi level. The valence and conduction bands in topological semimetals can touch at either discrete points or extended lines, forming Dirac/Weyl semimetals[13–16] and nodal line semimetals[1–3]. The band degeneracy points or lines in topological semimetals are also protected by symmetries and are thus

robust against external perturbations.

On the other hand, two-dimensional materials have also attracted broad scientific interest because of their exotic properties and possible applications in high-speed nano-devices[17]. Therefore, it is natural to ask the following question: do three-dimensional topological semimetals have counterparts in two-dimensional materials? The realization of two-dimensional topological semimetals will provide new platforms for the design of novel quantum devices at the nanoscale. For Dirac semimetals, a two-dimensional counterpart is graphene, when spin orbit coupling (SOC) is neglected[14, 15]. Two-dimensional nodal line semimetals[18] have recently been proposed in a honeycomb-kagome lattice[19] and monolayer transition metal-group VI compounds[20]. The nodal lines in both materials are protected by mirror reflection symmetry and require negligible SOC. However, the experimental realization of such structures in real materials is quite challenging; thus, it is necessary to search for new and realizable two-dimensional materials that host robust nodal lines.

In this work, we study monolayer Cu_2Si , which is composed of a honeycomb Cu lattice and a triangular Si lattice, as shown in Fig. 1(a). In the free-standing form, all Si and Cu atoms are coplanar[21] and thus mirror reflection symmetry with respect to the xy plane (M_z) is naturally expected; this is important for the existence of two-dimensional nodal lines. Importantly, the experimental synthesis of monolayer Cu_2Si is easy and has already been realized decades ago. One method to synthesize Cu_2Si is the direct growth of copper on Si(111)[22–24]. However, monolayer Cu_2Si forms a quasiperiodic superstructure on Si(111) without precise long range periodicity. Alternatively, a commensurate 1×1 structure of monolayer Cu_2Si has been synthesized on a Cu(111) surface using chemical vapor deposition (CVD) methods[25, 26]. As the 1×1 lattice of Cu_2Si approximately matches the $(\sqrt{3}\times\sqrt{3})R30^\circ$ superlattice of Cu(111), large domains of ordered Cu_2Si can form on the Cu(111) surface. However, previous investigations of Cu_2Si have primarily concentrated on the structural and chemical properties, and a detailed investigation of its band structures is still lacking. Here, our comprehensive theoretical calculations show the existence of two Dirac nodal loops centred around the Γ point. The gapless nodal loops are protected by mirror reflection symmetry. These intriguing band structures have been directly observed by ARPES measurements of $\text{Cu}_2\text{Si}/\text{Cu}(111)$. Both nodal loops survive in the $\text{Cu}_2\text{Si}/\text{Cu}(111)$ system because of the weak substrate-overlayer interaction.

The band structures of freestanding Cu_2Si without SOC are shown in Fig. 1(b). Within 2 eV of the Fermi level, there are three bands: two hole-like bands (labelled α and β) and one electron-like band (labelled γ). All three bands form closed contours on the Fermi surface: a hexagon, a hexagram, and a circle, respectively, as shown in Fig. 1(e). Interestingly, we find that band γ crosses bands α and β linearly in all directions without opening of energy gaps, thus forming two concentric Dirac nodal loops centred around the Γ point (labelled NL1 and NL2). In Fig. 1(f), we present the momentum distribution of gapless nodal points in the Brillouin zone, which shows a hexagon (NL1) and a hexagram

(NL2), respectively.

It is natural to ask whether the two gapless Dirac nodal loops in Cu_2Si are symmetry-protected or just an accidental band touching. To answer this question, we calculated the M_z parity of each band without SOC and find that the parity of band γ is opposite to that of bands α and β , as indicated by the “+” and “-” in Fig. 1(b). The opposing M_z parities indicate that band γ does not couple with bands α and β , and therefore both Dirac nodal loops remain gapless. This result provides strong evidence that the two gapless nodal loops are protected by mirror reflection symmetry.

After including SOC, each band is double-degenerate and the two degenerate bands have opposing M_z parity. As a result, the mirror reflection symmetry cannot protect the nodal loops anymore. Along the preceding Dirac nodal loops, the bands with the same parity will couple with each other, resulting in the opening of band gaps. The calculated band structures with SOC clearly show that the nodal lines are fully gapped [Figs. 1(c), 1(g), and 1(h)]. However, the size of the SOC gap is quite small because of the weak intrinsic SOC strength in Cu_2Si . After artificially increasing the SOC strength, the size of the gap increases accordingly, as shown in Fig. 1(d). These results show that mirror reflection symmetry only protects the Dirac nodal loops in the absence of SOC.

To further validate the role of mirror reflection symmetry in the protection of the gapless nodal loops, we introduce artificial perturbations to break the mirror reflection symmetry. The first method involves the introduction of buckling in the honeycomb Cu lattice while keeping the Si atoms unchanged, as schematically shown in the upper panel of Fig. 2(a). This kind of buckling in a honeycomb lattice is similar to the intrinsic buckling in silicene and germanene, with neighbouring atoms buckled upwards and downwards, respectively[27]. The second method to break the mirror reflection symmetry involves shifting the Si atoms downwards, as schematically shown in the bottom panel of Fig. 2(a). Our calculated band structures show that both nodal lines are gapped except the remaining gapless Dirac points along the Γ -M and Γ -K directions [Figs. 2(b) and 2(c)]. These results confirm that the two gapless nodal loops are protected by the mirror reflection symmetry. The remaining gapless Dirac cones may be protected by other crystal symmetries, which calls for further theoretical studies.

To directly confirm the intriguing nodal loop properties in Cu_2Si , we performed high-resolution ARPES to measure its band structures. We synthesized monolayer Cu_2Si by directly evaporating atomic Si on Cu(111) in an ultrahigh vacuum. This sample preparation method is superior to the previously reported CVD methods[25, 26], as it can avoid exotic impurities introduced by the gases. The as-prepared Cu_2Si sample is of high quality (see the Supplementary Information for details) and is thus suitable for the high-resolution ARPES measurements.

Monolayer Cu_2Si forms a $(\sqrt{3} \times \sqrt{3})\text{R}30^\circ$ superstructure with respect to the Cu(111)- 1×1 lattice, in agreement with previous reports[25, 26]. A schematic drawing of the Brillouin zones of Cu_2Si and Cu(111) is shown in Fig. 3(a). In Figs. 3(b)-3(e), we show the evolution of constant energy contours (CECs) with

binding energies. Several closed contours centred at the Γ point can be seen: one hexagon, one hexagram, and one circle, despite the anisotropic intensities resulting from the matrix element effects. These bands agree well with bands α , β , and γ from our calculations [Fig. 1(e)]. With increasing binding energies, the sizes of the hexagon and hexagram increase, while the size of the circle decreases. In particular, the circle is larger than the hexagon and hexagram at the Fermi level and becomes smaller at binding energies higher than 1.0 eV, indicating the existence of two nodal loops centred at the Γ point.

In Fig. 3(f), we show the ARPES intensity plots measured along the Γ -K direction. The band crossings, i.e., the nodal lines, are clearly observed at both sides of the Γ point (indicated by the black arrows), in agreement with the evolution of the CECs from Fig. 3. The band crossing is located at deeper binding energy compared with the freestanding Cu_2Si [Fig. 1(b)], which might originate from the electron doping of the metallic $\text{Cu}(111)$ substrate. Furthermore, linear dispersion is observed near the nodal lines, in agreement with our theoretical calculation results. These results show that the quasiparticles in Cu_2Si are Dirac nodal line fermions. Because of the small separation of α and β bands along the Γ -K direction, the two bands are not clearly resolved in Fig. 3(f). However, from the momentum distribution curves (MDCs) taken at $E_B=1.3$ eV [Fig. 3(i)], we find that the peaks are asymmetric (indicated by the blue and orange arrows), indicating the existence of two bands, i.e., α and β bands. To further confirm the intriguing band structures in Cu_2Si , we show the ARPES intensity plots along a series of parallel momentum cuts in the Γ -K direction, as indicated in Fig. 4(a). From cut 1 to cut 10, band β first moves closer to band α until $k_y=0$ (cut 3), and then separates again. We note that cut 8 is measured along one edge of the hexagonal NL1, so one can see a relatively flat band near $E_B=1.0$ eV (indicated by a black arrow). These results agree well with our calculated band structures and thus confirm the existence of two Dirac nodal loops in Cu_2Si .

As Cu_2Si is only one atomic layer thick, all three bands are expected to have two-dimensional characteristics, i.e., no k_z dispersion, which can be confirmed by ARPES measurements with different photon energies. In Figs. 3(f)-3(g), we show the ARPES intensity plots along the Γ -K direction measured with three different photon energies. From the MDCs taken at $E_B=1.3$ eV, the peak positions do not shift with the change in photon energies, as shown in Fig. 3(i). The photon energy-independent behaviour indicates no k_z dispersion for the three bands, in agreement with their two-dimensional characteristics. The intensity variance of these bands originates from the matrix element effects in the photoemission process. On the other hand, the bulk bands of $\text{Cu}(111)$ are expected to be folded to the first Brillouin zone of Cu_2Si because of the Umklapp scattering of the $(\sqrt{3} \times \sqrt{3})\text{R}30^\circ$ superlattice. However, we did not observe the folded bulk bands of $\text{Cu}(111)$ within our experimental resolution. This result indicates a weak interaction between Cu_2Si and $\text{Cu}(111)$ that results in the negligible intensity of the folded bands.

It should be noted that the mirror reflection symmetry in Cu_2Si is indeed broken when it is prepared on the $\text{Cu}(111)$ surface. This is because one side of Cu_2Si is vacuum, while the other side is the $\text{Cu}(111)$

substrate. The interaction with the substrate could open a band gap at the nodal lines because of the breaking of mirror reflection symmetry. However, we do not find a clear signature of gap opening in our ARPES measurements, which is another evidence for the weak interaction of Cu_2Si and the $\text{Cu}(111)$ substrate. Indeed, previous experimental and theoretical works have already confirmed that the surface Cu_2Si layer remains approximately planar on $\text{Cu}(111)$ [28, 29] and the electronic states are strongly localized in the surface Cu_2Si layer[30], which indicates that the mirror reflection symmetry is preserved to a large extent. As a result, no obvious gap opens at the Dirac nodal lines within our experimental resolution. As we have discussed in Fig. 1(c), SOC can also lead to gap opening at the nodal lines, but the intrinsic SOC in Cu_2Si is too weak to induce detectable gaps.

Our theoretical and experimental results have unambiguously confirmed the existence of two concentric Dirac nodal loops in monolayer Cu_2Si . These nodal loops are protected by the mirror reflection symmetry and thus robust against symmetry conserving perturbations. These results not only extend the concept of Dirac nodal lines from three- to two-dimensional materials, but also provide a new platform to realize novel devices at the nanoscale. As copper has already been widely used for the preparation and subsequent transfer of graphene, we expect that monolayer Cu_2Si will be able to be transferred to insulating substrates, which is crucial for future transport measurements and device applications. On the other hand, although the breaking of mirror reflection symmetry will destroy the global Dirac nodal loops, our theoretical calculations have found the formation of gapless Dirac cones along the Γ -M and Γ -K directions (Fig. 2). This result suggests the possibility of tuning the Dirac states in Cu_2Si by controllable breaking of the mirror reflection symmetry, which might be realized by selecting appropriate substrates.

Methods

Experiments. The sample preparation and photoemission measurements were performed at BL-9A of HiSOR at Hiroshima University and the VUV photoemission beamline of the Elettra synchrotron at Trieste. Single-crystal $\text{Cu}(111)$ was cleaned by repeated sputtering and annealing cycles. Monolayer Cu_2Si was prepared by directly evaporating Si on $\text{Cu}(111)$ while keeping the substrate at approximately 500 K. The structure of Cu_2Si was confirmed by the appearance of sharp $(\sqrt{3} \times \sqrt{3})\text{R}30^\circ$ low-energy electron diffraction (LEED) patterns. The pressure during growth was less than 1×10^{-7} Pa. After preparation, the sample was directly transferred to the ARPES chamber without breaking the vacuum. During the ARPES measurements, the sample was kept at 40 K. The energy resolution was better than 20 meV. The pressure during measurements was below 2×10^{-9} Pa.

Calculations. Our first-principles calculations were carried out using VASP (Vienna ab-initio simulation package)[31] within the generalized-gradient approximation of the Perdew, Burke, and Ernzerhof[32] exchange-correlation potential. A cutoff energy of 450 eV and a k-mesh of $27 \times 27 \times 1$ were chosen for self-consistent-field calculations. The lattice constant of 4.123 Å was obtained from the

experimental value, and the thickness of vacuum was set to 18 Å, which is adequate to simulate two-dimensional materials. The convergence criteria of total energy and the force of each atom were 0.001 eV and 0.01 eV/Å, respectively. The spin-orbital effect was considered in part of our calculations.

Acknowledgements

We thank Professor X. J. Zhou for providing the Igor macro to process the ARPES data. This work was supported by the Ministry of Education, Culture, Sports, Science and Technology of Japan (Photon and Quantum Basic Research Coordinated Development Program), the MOST of China (Grant Nos. 2014CB920903, 2016YFA0300600, 2013CBA01601, and 2016YFA0202300), the NSF of China (Grant Nos. 11574029, 11225418, 11674366, and 11674368), the Strategic Priority Research Program of the Chinese Academy of Sciences (Grant No. XDB07020100), and the US Department of Energy (DOE), Office of Science (OS), Office of Basic Energy Sciences, Division of Materials Science and Engineering (Grant No. DE-FG02-07ER46383).

* Electronic address: lchen@iphy.ac.cn

† Electronic address: ygyao@bit.edu.cn

‡ Electronic address: imatsuda@issp.u-tokyo.ac.jp

- [1] Burkov, A. A., Hook, M. D. & Balents, L. Topological nodal semimetals. *Phys. Rev. B* **84**, 235126 (2011).
- [2] Xu, G., Weng, H., Wang, Z., Dai, X. & Fang, Z. Chern semimetal and the quantized anomalous Hall effect in HgCr₂Se₄. *Phys. Rev. Lett.* **107**, 186806 (2011).
- [3] Fang, C., Chen, Y., Kee, H.-Y. & Fu, L. Topological nodal line semimetals with and without spin-orbital coupling. *Phys. Rev. B* **92**, 081201 (R) (2015).
- [4] Huh, Y., Moon, E.-G. & Kim, Y. B. Long-range Coulomb interaction in nodal-ring semimetals. *Phys. Rev. B* **93**, 035138 (2016).
- [5] Rhim, J.-W. & Kim, Y. B. Landau level quantization and almost flat modes in three-dimensional semimetals with nodal ring spectra. *Phys. Rev. B* **92**, 045126 (2015).
- [6] Wu, Y., Wang, L.-L., Mun, E., Johnson, D. D., Mou, D., Huang, L., Lee, Y., Bud'ko, S. L., Canfield, P. C. & Kaminski, A. Dirac node arcs in PtSn₄. *Nat. Phys.* **12**, 667-671 (2016).
- [7] Bian, G. *et al.* Topological nodal-line fermions in spin-orbit metal PbTaSe₂. *Nat. Commun.* **7**, 10556 (2016).
- [8] Bian, G. *et al.* Drumhead surface states and topological nodal-line fermions in TiTaSe₂. *Phys. Rev. B* **93**, 121113 (R) (2016).
- [9] Schoop, L. M., Ali, M. N., Straßer, C., Topp, A., Varykhalov, A., Marchenko, D., Duppel, V., Parkin, S. S. P., Lotsch, B. V. & Ast, C. R. Dirac cone protected by non-symmorphic symmetry and three-dimensional Dirac line node in ZrSiS. *Nat. Commun.* **7**, 11696 (2016).
- [10] Neupane, M., *et al.* Observation of topological nodal fermion semimetal phase in ZrSiS. *Phys. Rev. B* **93**, 201104 (R) (2016).
- [11] Hasan, M. Z. & Kane, C. L. Colloquium: Topological insulators. *Rev. Mod. Phys.* **82**, 3045-3067 (2010).
- [12] Qi, X.-L. & Zhang, S.-C. Topological insulators and superconductors. *Rev. Mod. Phys.* **83**, 1057-1110 (2011).

- [13] Young, S. M., Zaheer, S., Teo, J. C. Y., Kane, C. L., Mele, E. J. & Rappe, A. M. Dirac semimetal in three dimensions. *Phys. Rev. Lett.* **108**, 140405 (2012).
- [14] Wang, Z., Sun, Y., Chen, X.-Q., Franchini, C., Xu, G., Weng, H., Dai, X. & Fang, Z. Dirac semimetal and topological phase transitions in A_3Bi ($A=Na, K, Rb$). *Phys. Rev. B* **85**, 195320 (2012).
- [15] Liu, Z. K., *et al.* Discovery of a three-dimensional topological Dirac semimetal, Na_3Bi . *Science* **343**, 864-867 (2014).
- [16] Xu, S., *et al.* Discovery of a Weyl fermion semimetal and topological Fermi arcs. *Science* **349**, 613-617 (2015).
- [17] Xu, M., Liang, T., Shi, M. & Chen, H. Graphene-like two-dimensional materials. *Chem. Rev.* **113**, 3766-3798 (2013).
- [18] Li, L. & Araujo, M. A. N. Topological insulating phases from two-dimensional nodal loop semimetals. *Phys. Rev. B* **94**, 165117 (2016).
- [19] Lu, J. L., Luo, W., Li, X. Y., Yang, S. Q., Cao, J. X., Gong, X. G. & Xiang, H. J. Two-dimensional node-line semimetals in a honeycomb-kagome lattice. arXiv:1603.04596 (2016).
- [20] Jin, Y., Wang, R., Zhao, J., Zheng, C., Gan, L.-Y., Liu, J., Xu, H. & Tong, S. Y. A family group of two-dimensional node-line semimetals. arXiv:1608.05791 (2016).
- [21] Yang, L.-M., Bacic, V., Popov, I. A., Boldyrev, A. I., Heine, T., Frauenheim, T. & Ganz, E. Two-dimensional Cu_2Si monolayer with planar hexacoordinate copper and silicon bonding. *J. Am. Chem. Soc.* **137**, 2757-2762 (2015).
- [22] Chambers, S. A., Anderson, S. B. & Weaver, J. H. Atomic structure of the $Cu/Si(111)$ interface by high-energy core-level Auger electron diffraction. *Phys. Rev. B* **32**, 581-587 (1985).
- [23] Zegenhagen, J., Fontes, E., Grey, F. & Patel, J. R. Microscopic structure, discommensurations, and tiling of $Si(111)/Cu$ -“5 \times 5”. *Phys. Rev. B* **46**, 1860-1863 (1992).
- [24] Neff, H.-J., Matsuda, I., Hengsberger, M., Baumberger, F., Greber, T. & Osterwalder, J. High-resolution photoemission study of the discommensurate (5.55 \times 5.55) $Cu/Si(111)$ surface layer. *Phys. Rev. B* **64**, 235415 (2001).
- [25] Curson, N. J., Bullman, H. G., Buckland, J. R. & Allison, W. Interaction of silane with $Cu(111)$: Surface alloy and molecular chemisorbed phases. *Phys. Rev. B* **55**, 10819-10829 (1997).
- [26] Menard, H., Horn, A. B. & Tear, S. P. Methylsilane on $Cu(111)$, a STM study of the ($\sqrt{3}\times\sqrt{3}$) $R30^\circ$ - Cu_2Si surface silicide. *Surf. Sci.* **585**, 47-52 (2005).
- [27] Cahangirov, S., Topsakal, M., Akturk, E., Sahin, H. & Ciraci, S. Two- and one-dimensional honeycomb structures of silicon and germanium. *Phys. Rev. Lett.* **102**, 236804 (2009).
- [28] Shuttleworth, I. G., Fisher, C. J., Lee, J. J., Jones, R. G. & Woodruff, D. P. A NIXSW structural investigation of the ($\sqrt{3}\times\sqrt{3}$) $R30^\circ$ - Cu_2Si surface alloy phase formed by SiH_4 reaction with $Cu(111)$. *Surf. Sci.* **491**, L645-L650 (2001).
- [29] Shuttleworth, I. G. Deduction of a three-phase model for the ($\sqrt{3}\times\sqrt{3}$) $R30^\circ$ - $Cu_2Si/Cu(111)$ surface alloy. *Appl. Surf. Sci.* **256**, 636-639 (2009).
- [30] Shuttleworth, I. G. Investigation of the ($\sqrt{3}\times\sqrt{3}$) $R30^\circ$ - $Cu_2Si/Cu(111)$ surface alloy using DFT. *Appl. Surf. Sci.* **257**, 6792-6798 (2011).
- [31] Kresse, J. & Furthmüller, J. Efficient iterative schemes for ab initio total-energy calculations using a plane-wave basis set. *Phys. Rev. B* **54**, 11169-11186 (1996).
- [32] Perdew, J. P., Burke, K. & Ernzerhof, M. Generalized gradient approximation made simple. *Phys. Rev. Lett.* **77**, 3865-3868 (1996).

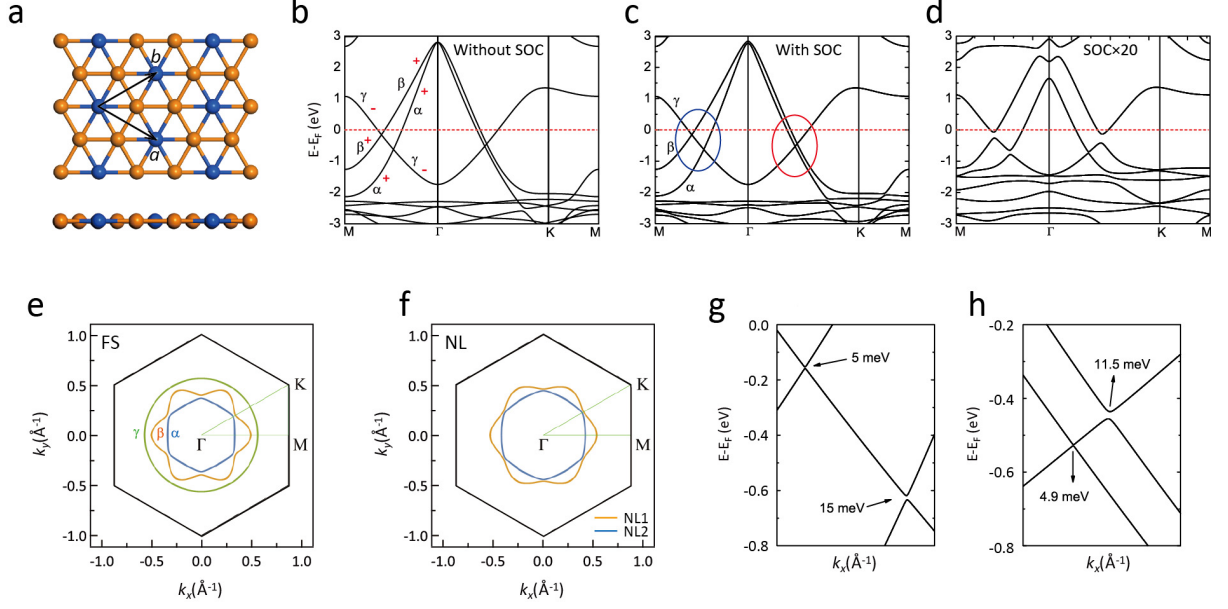


FIG. 1: **Atomic and band structures of free-standing Cu_2Si .** (a) Top and side view. The orange and blue balls represent Cu and Si atoms, respectively. (b,c) Calculated band structures of Cu_2Si with and without spin-orbit coupling (SOC), respectively. The vertical axis $E - E_F$ corresponds to $-E_B$, where E_B is the binding energy. For simplicity, we label the three bands that cross the Fermi level α , β , and γ , respectively. The parity of mirror reflection symmetry for each band is labelled “+” and “-” in (b). The zoom-in band structures in the blue and red ellipses are shown in (g) and (h). (d) Band structure of Cu_2Si after artificially increasing the intrinsic SOC by 20 times. (e) Fermi surface of Cu_2Si without SOC. The blue, orange, and green lines correspond to bands α , β , and γ , respectively. (f) Momentum distribution of the nodal loops: NL1 (blue) and NL2 (orange). (g,h) Zoom-in band structures in the blue and red ellipses in (c), which clearly show the SOC-induced gaps.

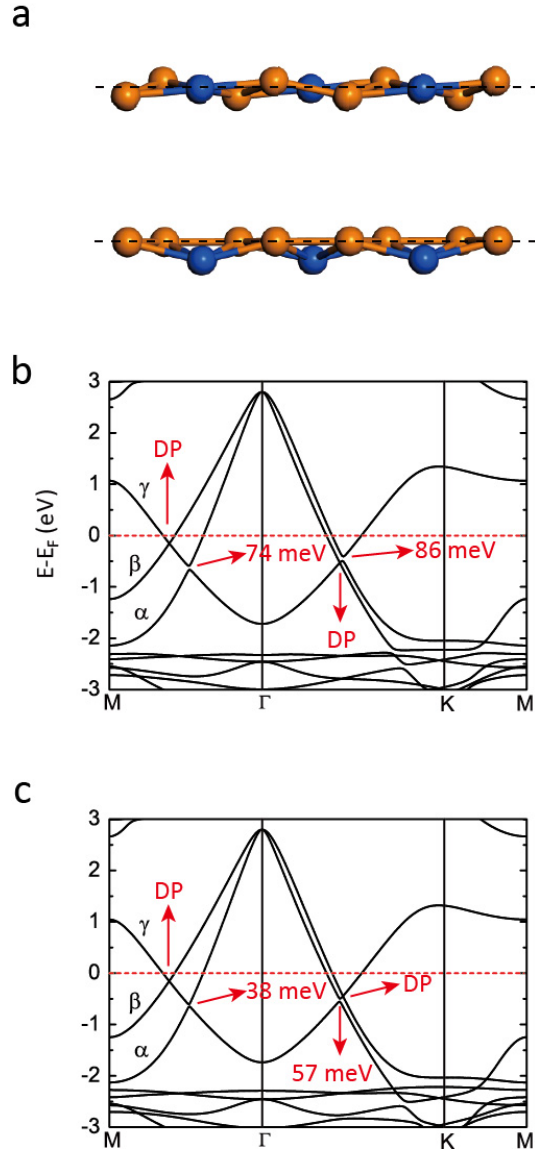


FIG. 2: **Band structures of Cu₂Si without SOC after breaking the mirror reflection symmetry.** (a) Two configurations that break the mirror reflection symmetry in Cu₂Si. Top panel: the neighbouring Cu atoms have a 0.1 Å buckling while the Si atoms remain in-plane; bottom panel: the Si atoms are shifted 0.1 Å downwards. The shift of atoms is enlarged for clarity. The horizontal dashed lines indicate the original plane where all atoms were located before the shift. (b,c) Calculated band structures for the two configurations in (a). The nodal lines are gapped, except for one gapless Dirac point (DP) along the Γ -M and Γ -K directions. The sizes of the gaps are indicated in (b) and (c).

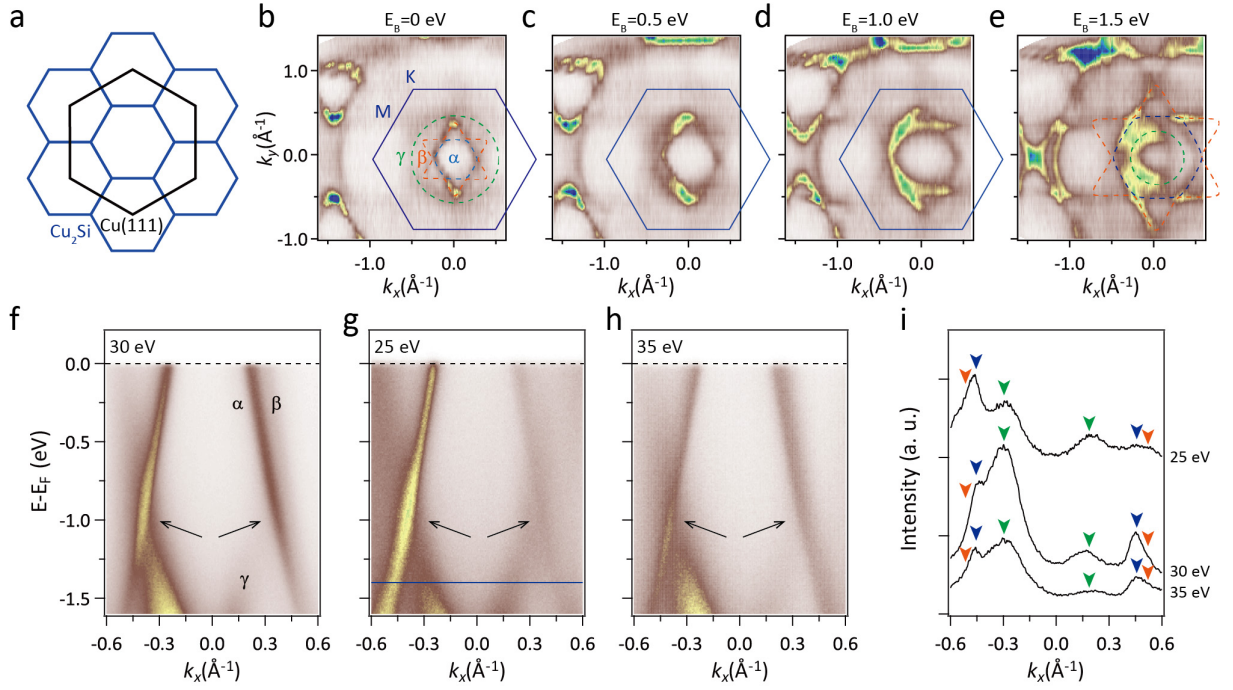


FIG. 3: **ARPES results for monolayer Cu_2Si on $\text{Cu}(111)$.** (a) Schematic drawing of the Brillouin zones of Cu_2Si (blue hexagons) and $\text{Cu}(111)$ (black hexagon). As the lattice of Cu_2Si is $(\sqrt{3} \times \sqrt{3})R30^\circ$ with respect to the $\text{Cu}(111)$ - 1×1 lattice, the K point of $\text{Cu}(111)$ is located at the Γ point of the second Brillouin zone of Cu_2Si . (b-e) Constant energy contours measured using 30-eV photons. Three closed contours have been observed: a hexagon, a hexagram, and a circle, as indicated by the dashed lines. (f-h) ARPES intensity plots along the Γ -K direction with different photon energies: 30 eV, 25 eV, and 35 eV, respectively. The black arrows mark the position of the crossing points. (i) Momentum distribution curves taken at $E_B = 1.3$ eV [blue line in (g)] using different photon energies. The blue, orange, and green arrows indicate the positions of the peaks that correspond to bands α , β , and γ , respectively. The positions of the peaks do not change with photon energy, in agreement with their two-dimensional characteristics.

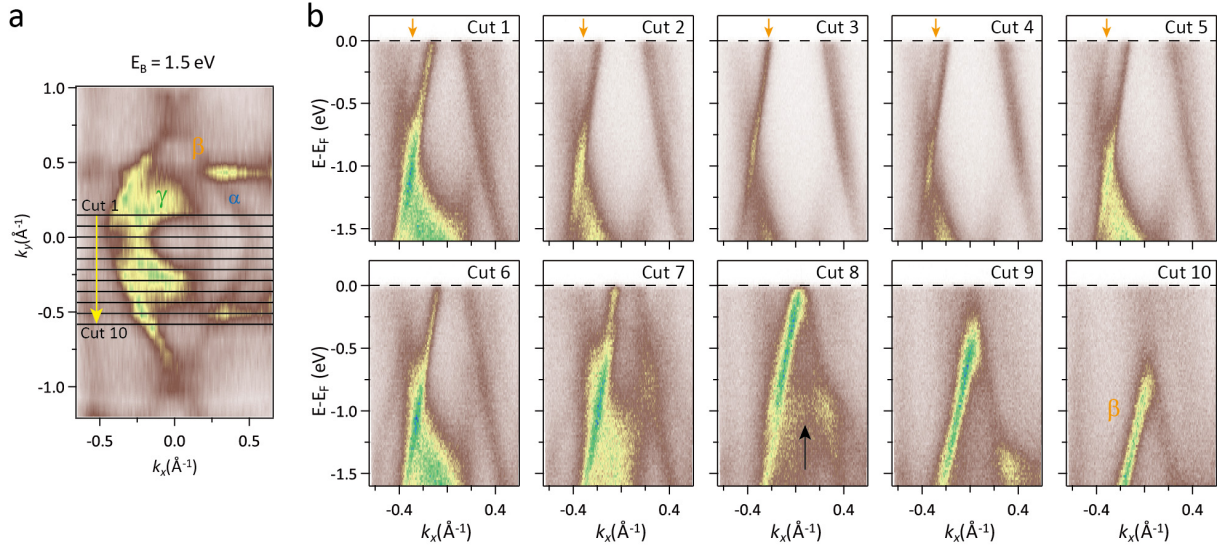


FIG. 4: **Detailed band structures of Cu_2Si on $\text{Cu}(111)$.** (a) Constant energy contour taken at $E_B=1.5$ eV. The black lines (cut 1 to cut 10) indicate the positions where the ARPES intensity plots in (b) are taken. (b) ARPES intensity plots measured along cut 1 to cut 10. The orange arrows indicate the evolution of band β . The black arrow in cut 8 indicates a flat band that originates from NL1.